Structural analysis of rubble-pile asteroids applied to collisional evolution

Yang Yu[1] (✉), **Derek C. Richardson**[2], **and Patrick Michel**[3]

1. *School of Aeronautic Science and Technology, Beihang University, Beijing 100191, China*
2. *Department of Astronomy, University of Maryland, College Park MD 20740-2421, USA*
3. *Observatoire de la Côte d'Azur, UMR 7293 Lagrange/CNRS, 06304 Nice Cedex 4, France*

ABSTRACT

Solar system small bodies come in a wide variety of shapes and sizes, which are achieved following very individual evolutional paths through billions of years. Nevertheless, some common mechanisms can still be found during these processes, e.g., rubble-pile asteroids tend towards fluid equilibrium as they are reshaped by external disturbances. This paper focuses on the reshaping process of rubble-pile asteroids driven by meteorite impacts. A mesoscale cluster of solid spheres is employed as the principal model for a rubble-pile asteroid, for which little is actually known about their interior structure. We take this simple model as a rough guide to the qualitative aspects of the reshaping processes, and it can reveal, to some degree, the inner workings of rubble-pile asteroids. In our study, numerous possible equilibrium configurations are obtained via Monte Carlo simulation, and the structural stability of these configurations is determined via eigen analysis of the geometric constructions. The eigen decomposition reveals a connection between the cluster's reactions and the types of external disturbance. Numerical simulations are performed to verify the analytical results. The gravitational N-body code `pkdgrav` is used to mimic the responses of the cluster under intermittent non-dispersive impacts. We statistically confirm that the stability index I_S, the total gravitational potential P_G, and the volume of inertia ellipsoid V_E show consistent tendency of variation. A common regime is found in which the clusters tend towards crystallization under intermittent impacts, i.e., only the configurations with high structural stability survive under the external disturbances. The results suggest the trivial non-disruptive impacts might play an important role in the rearrangement of the constituent blocks, which may strengthen these rubble piles and help to build a robust structure under impacts of similar magnitude. The final part of this study consists of systematic simulations over two parameters, the projectile momentum and the rotational speed of the cluster. The results show a critical value exists for the projectile momentum, as predicted by theory, below which all clusters become responseless to external disturbances; and the rotation proves to be significant for it exhibits an "enhancing" effect on loose-packed clusters, which coincides with the observation that several fast-spinning asteroids have low bulk densities.

✉ yuyang.thu@gmail.com

TSINGHUA UNIVERSITY PRESS   Springer

1 Introduction

There is abundant evidence that most asteroids between ∼100 m and ∼100 km in size are gravitational aggregates of boulders, whether born as loosely consolidated structures or formed from the remains of shattered larger bodies [1]. The constitution of asteroids proved to have a significant role during their subsequent evolution [2,3]. Generally, rubble-pile asteroids are very responsive to close planetary tides because of the near-strengthless interiors [4, 5], and present good resistance to further disruption from meteorite impacts due to the high energy diffusion of their structures [6]. Observations have shown reshaping marks of rubble-pile asteroids due to the disturbances during geological processes. More than 20 asteroid families in the main belt suggest a collisional origin in which large impactors shattered the parent body and the fragments reaccumulated to form the large family members [7]. Comet breakups, e.g., Comet D/Shoemaker–Levy 9 at Jupiter, showed the tidal disruption effects of planetary tides during close encounter [8,9]. Richardson *et al.* [10] used *N*-body simulations to explore the possible outcomes of tidal encounters of rubble-pile asteroids with the Earth, and found similar fragment trains are created for severe disruptions.

In reality, the violent processes have statistically low probability, while moderate disturbances, such as weak tidal encounters or non-dispersive impacts from micrometeorites, seem to be more common experiences for most rubble-pile asteroids. These events can lead to seismic shaking and slight distortion of the interior structure. It was found that the double-lobed shape of several asteroids such as (4769) Castalia, (2063) Bacchus, (4179) Toutatis, and (216) Kleopatra could be formed by the gentle mutual reactions between similar-sized bodies following a tidal breakup or a low-speed collision [10–12]. Accordingly, the continual low-energy events may have the potential to modify the interior structure of rubble-pile asteroids in quasi-equilibria. Early work suggested that asteroids may have fluid equilibrium shapes [13], but more recent observations show that this is generally not the case [14]. In fact, asteroids of ∼100 km or smaller are likely formed of discrete blocks with different sizes and shapes, which provides some shear strength that prevents the overall shape from coming to fluid equilibrium [15, 16]. Tanga

et al. [17] proposed that a general mechanism exists to produce the observed shape distribution, that the fragmented structure could progressively reshape via gradual rearrangement of the constituent blocks due to external forces, such as planetary tides, non-dispersive impacts, etc. *N*-body simulations were employed to investigate the equilibration of rubble piles based on a 4-dimensional parametric space, and the results showed external factors can break the interlocking of the rubble piles and drive them to asymptotically evolve toward fluid equilibrium.

It is interesting to develop this idea further, to explore how the reshaping process of a rubble pile depends on its interior structure, i.e., can we figure out the structural stability and collisional responses of a rubble pile from its configuration? One approach is to start with a basic model. We choose a simple soft-sphere cluster to mimic the real rubble pile, with all blocks modeled as solid spheres [18,19]. This is not for accurate reproduction of the asteroid constitution but serves as a bridge to understand the natural evolution of rubble-pile asteroids during intermittent disturbances. Richardson *et al.* [1] proposed a scheme to place the asteroid in a two-parameter diagram of porosity and relative tensile strength, defining eight typical asteroid structures: monolithic, fractured, shattered, shattered with rotated components, rubble pile, coherent rubble pile, weak-and-porous, and strong-and-porous. One benefit of this classification is it helps distinguish the responses of different types of interior structures during geological processes. In this study, we focus on clusters of tens of spheres based on the following rationale: first, the mesoscale clusters can be regarded as representative of some (perhaps many) asteroids that have not been fully shattered, and their overall shapes are largely determined by some big components; second, the rubble piles composed of big constituents behave more like discrete bodies than fluid bodies and provide a good approximation to real rubble-pile asteroids; third, rubble piles of tens of spheres may have been representative for the complex dynamics (though not as complex as the aggregates of more spheres) and possess various possible equilibrium configurations. This diversity of this simple case essentially relies on the nature of sphere clusters, thus it holds even when some complex interactions, such as the geometrical locking and static friction, are omitted.

This paper presents a quantitative estimation of the

structural stability of the rubble-pile model, which is then applied to the investigation of the responses of rubble-pile asteroids to different disturbances. Numerical simulations are performed using the code `pkdgrav`, a gravitational N-body code which is well suited for discrete material. Section 2 introduces the theoretical analysis of structural stability of a rubble-pile configuration, along with a numerical example as validation. Section 3 describes the three groups of simulations we performed, including choice of parameters used. Section 4 discusses the results of these numerical experiments. We validate the results of our structural analysis in two ways: to check the responses of numerous sample clusters statistically, and to track the detailed behaviors of a specified cluster.

2 Structural analysis of equilibrium cluster

2.1 Representation of equilibrium cluster

The mesoscale clusters are obtained through an assembly of equal-sized soft spheres. No cohesion or friction is considered here, i.e., the spheres stay together via mutual gravity alone. Initialized as a random cloud of particles in space, the spheres evolve gradually into an equilibrium cluster due to the frictional damping and collisional dissipation. Consider a cluster of N spheres; the mass and radius of each sphere are defined as m and R, and $\boldsymbol{r}_i$ is the position vector of sphere i. Define the delta function:

$$\delta_{i,j} = \begin{cases} 1, & \text{if } |\boldsymbol{r}_i - \boldsymbol{r}_j| < 2R \\ 0, & \text{if } |\boldsymbol{r}_i - \boldsymbol{r}_j| \geqslant 2R \end{cases} \quad (1)$$

and represent the position of sphere $\boldsymbol{r}_i$ in the central principal frame (CPF), which is defined with the origin at the system mass center, and x-, y-, z-axes aligned along the small, medium, and large principal axes of inertia, respectively. Note that CPF exists only if the cluster is equilibrated. The equilibrium equation of sphere i is given by Eq. (2):

$$\sum_{j \neq i} \boldsymbol{G}_{i,j} + \sum_{j \neq i, \delta_{i,j}=1} \boldsymbol{C}_{i,j} + \Omega^2 \boldsymbol{r}_i - (\boldsymbol{\Omega} \cdot \boldsymbol{r}_i)\boldsymbol{\Omega} = \boldsymbol{0},$$

$$i = 1, 2, \ldots, N \quad (2)$$

$$\boldsymbol{G}_{i,j} = \frac{Gm^2}{|\boldsymbol{r}_i - \boldsymbol{r}_j|^3} (\boldsymbol{r}_j - \boldsymbol{r}_i) \quad (3)$$

$$\boldsymbol{C}_{i,j} = -K_{\text{n}} \left(1 - \frac{2R}{|\boldsymbol{r}_i - \boldsymbol{r}_j|}\right) (\boldsymbol{r}_i - \boldsymbol{r}_j) + K_{\text{t}} \boldsymbol{S}_{i,j} \quad (4)$$

Equations (3) and (4) define respectively the gravitational attraction and contact force on sphere i from sphere j. And $\boldsymbol{S}_{i,j}$ indicates the tangential displacement between spheres i and j (see Ref. [19] for a detailed description). The angular velocity $\boldsymbol{\Omega}$ is a constant vector if the cluster is equilibrated. G indicates the gravitational constant, and K_{n}, K_{t} indicate the constants for the normal spring and tangential spring, respectively. Then every solution $\boldsymbol{x}$ to this $3N$-dimensional equation presents a possible equilibrium configuration of this cluster, and is called the configuration for short, i.e.

$$\boldsymbol{x} = [\boldsymbol{r}_1, \boldsymbol{r}_2, \ldots, \boldsymbol{r}_N]^{\text{T}} \quad (5)$$

and as a canonical expression of the cluster in CPF, $\boldsymbol{x}$ represents a unique structure of the cluster, independent of the translation/rotation with respect to the inertia frame. Denoting the left-hand side of Eq. (2) as $\boldsymbol{F}_i$, with the three components $F_{i,x}, F_{i,y}, F_{i,z}$, Eq. (2) can be written as

$$F_{i,x} = 0, F_{i,y} = 0, F_{i,z} = 0, \quad i = 1, 2, \ldots, N \quad (6)$$

The Jacobi matrix of Eq. (6) yields:

$$\boldsymbol{M} = \left[\frac{\partial F_{1,x}}{\partial \boldsymbol{x}}, \frac{\partial F_{1,y}}{\partial \boldsymbol{x}}, \frac{\partial F_{1,z}}{\partial \boldsymbol{x}}, \frac{\partial F_{2,x}}{\partial \boldsymbol{x}}, \frac{\partial F_{2,y}}{\partial \boldsymbol{x}}, \right.$$
$$\left. \frac{\partial F_{2,z}}{\partial \boldsymbol{x}}, \ldots, \frac{\partial F_{N,x}}{\partial \boldsymbol{x}}, \frac{\partial F_{N,y}}{\partial \boldsymbol{x}}, \frac{\partial F_{N,z}}{\partial \boldsymbol{x}} \right] \quad (7)$$

The $3N \times 3N$ matrix $\boldsymbol{M}$ expresses the linear part of Eq. (2) and determines the local behavior of this dynamical system, i.e., the responses of the cluster after being disturbed from equilibrium configuration $\boldsymbol{x}$, as shown by the linear system of Eq. (8):

$$\begin{bmatrix} \dot{\boldsymbol{y}} \\ \ddot{\boldsymbol{y}} \end{bmatrix} = \begin{bmatrix} \boldsymbol{0} & \boldsymbol{I} \\ \boldsymbol{M} & \boldsymbol{0} \end{bmatrix} \begin{bmatrix} \boldsymbol{y} \\ \dot{\boldsymbol{y}} \end{bmatrix} \quad (8)$$

where $\boldsymbol{y} = \delta\boldsymbol{x}$ is the disturbance around configuration $\boldsymbol{x}$, $\boldsymbol{0}$ is a $3N \times 3N$ zero matrix, and $\boldsymbol{I}$ is a $3N \times 3N$ identity matrix. The linear matrix of Eq. (8) (symbolized as $\boldsymbol{L}$) presents the transient response of the cluster under any type of disturbance, either on the position or on the velocity, which enables us to check the structural stability of given configuration $\boldsymbol{x}$ via eigen analysis of $\boldsymbol{L}$ [20]. In the remaining part of this section, we will detail this correlation with an example.

2.2 An example

A mesoscale cluster of 27 spheres is used as an example, which is strength-dominated in structure. The radius of the sphere is 30.0 m. The normal chondrite density ~ 2.7 g/cm^3 is adopted here and the overall dimension is ~ 300 m. To generate a configuration, spheres were randomly dispersed in a cubic region initially, and then they gathered under mutual gravity naturally and collapse to form an aggregate. Note that static friction in the equations of motion is omitted so that Eq. (8) describes a continuous differentiable system, i.e., the theory of linearized stability applies [21]. Further setting the tangential damping constant C_t and stiffness constant K_t both to zero, the lack of friction makes the soft-sphere system more fluid, so the possible resulting configurations should be concentrated around the fluid equilibrium. The rotational state of each single sphere is neglected because the librational motion is decoupled from the translational motion for spheres. 162 eigenvalues λ_i $(i = 1, \ldots, 162)$ of the linearized matrix $\boldsymbol{L}$ are calculated at a given equilibrium configuration $\boldsymbol{x}$.

Figure 1 illustrates the distribution of these eigenvalues (b) for given configuration (a). The 162 eigenvalues are distributed in three branches on the complex plane: the stable branch is composed of the negative real axis and the parabola symmetric about it; the critical branch is the imaginary axis; and the unstable branch is the positive real axis.

We confirm numerically the pattern of this distribution is a common characteristic of equilibrium configurations for any clusters (see also Section 4.1.2). And it is correlated with the mechanical nature of the soft-sphere element. To understand this, several points should be stated first:

(1) Eigenvalues λ_i are in pairs, e.g., conjugate complex numbers (stable branch), conjugate imaginary numbers (critical branch), and opposite real numbers (positive value on unstable branch, negative value on stable branch). In physics, conjugate complex λ_i with negative real part indicates the disturbed cluster experiences damped shaking to revert to the original configuration; conjugate imaginary λ_i indicates constant-amplitude shaking; negative real λ_i indicates directly reverting to the original configuration; and positive λ_i indicates leaving the original configuration, i.e., the disturbance is irreversible
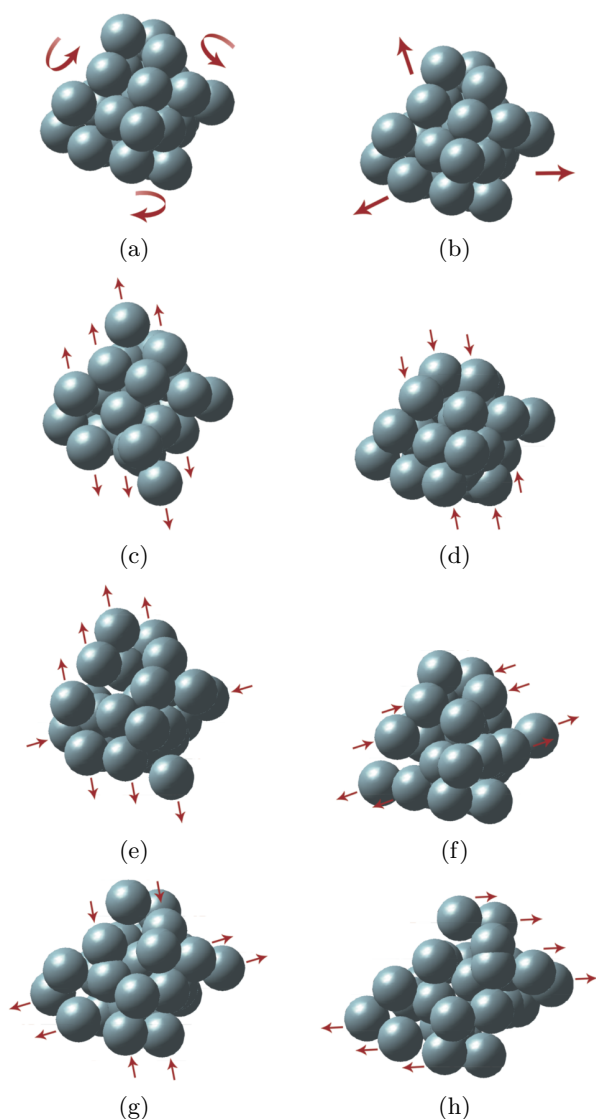

(a) Configuration

(b) Distribution of eigenvalues
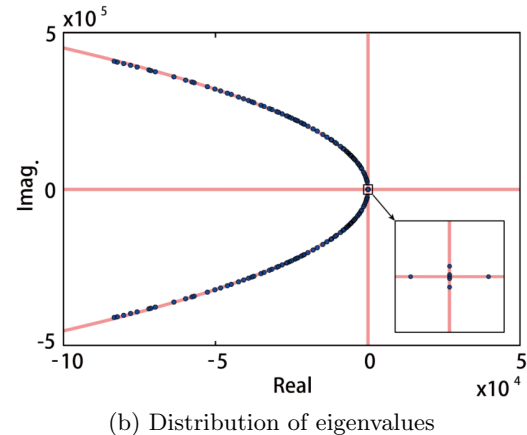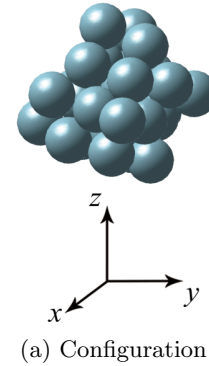
Fig. 1 Distribution of eigenvalues λ_i on the complex plane (unit: s^{-1}) for given equilibrium configuration. (a) shows the configuration of given cluster, and (b) shows λ_i on the complex plane. The light red lines indicate three feasible branches, and the solid circles indicate coordinates of λ_i. The floating box in (b) shows an enlarged view of the neighborhood around the origin.

for given cluster.

(2) The reason for the parabolic stable branch of λ_i is the linear mechanical properties in the soft-sphere element, i.e., the constant damping coefficient C_n and the stiffness coefficient K_n. For an arbitrary sphere of the cluster, the damping force and elastic force acting on it accumulate with the number of neighboring spheres, thus the ratio keeps constant and equals C_n/K_n. Also we notice the real part of eigenvalue $\mathrm{Re}\,(\lambda_i) \propto C_n$ and the imaginary part $\mathrm{Im}\,(\lambda_i) \propto \sqrt{K_n}$ [22]; therefore, $\mathrm{Re}\,(\lambda_i)$ and $\mathrm{Im}\,(\lambda_i)^2$ always change in proportion.

(3) Six zero eigenvalues always exist for the cluster, which correspond to the six degrees of freedom for the rigid motion, i.e., coherent translation or rotation of the given equilibrium configuration. Evidently, these types of disturbances lead to no response of the cluster configuration.

In summary, the eigenvalue set $\{\lambda_i\}$ actually measures the stability and stability margin of a configuration for

a given cluster. In Fig. 1, most λ_i are located at the stable branches and only one is located at the unstable branch, with a very small real part, so this largely indicates a stable configuration in CPF. Furthermore, the eigenvector ϕ_i associated with λ_i describes the type of disturbance corresponding to λ_i. We examined the 162 eigenvectors by exaggerating the magnitude of the disturbances. Figure 2 illustrates several typical and representative types of disturbances indicated by these eigenvectors.

It is notable that the disturbances shown in Fig. 2 are not based on a complete categorization; instead, they are chosen as a summarry of typical reconfiguring patterns. For example, cases (c)–(g), each represent tens of different ϕ_i, with similar disturbance types. Specifically, (a) indicates speeding up the rotation, corresponding to 6 pure imaginary λ_i, i.e., the critical stable state of a rotating cluster; with similar disturbance types (b) denotes the rigid translation mode corresponding to 6 zero λ_i, indicating the clusters under translational disturbance are all stable; (c)–(g) denote complex λ_i at stable branches, including simple tension/compression (c, d), and coupled tension and compression (e, f, g), all produced in reflection symmetry; (h) denotes the shearing mode corresponding to a λ_i at the unstable branch, suggesting that the cluster would be much more susceptible under shearing disturbance compared to other types. Also, the magnitude of λ_i in stable branches suggests the extent of structural stability of the cluster, e.g., the compression (d) has λ_i with larger magnitude than the tension (c) and accordingly the compressed cluster gains a faster recovery from the disturbance.

As a related aside, this example is not deliberately chosen. As a random equilibrium cluster, it provides a simplistic model to enable the eigenvector analysis, and interesting results can be presented in an intuitional way. The number of the disturbance forms depends highly on the interior structure of the equilibrium cluster (the force chain), and things will go complex when a size distribution of the spheres is considered. As a usual means to verify the eigen analysis, the numeric results meet the theoretical predictions well, which is the basis for applying this method in the following data processing of Section 4.

Fig. 2   8 representative forms of disturbances corresponding to eigenvectors ϕ_i. The snapshots are taken in CPF, and the reconfiguring effects are exaggerated for better visibility. The small arrows denote the displacement of spheres, the thick arrows denote coherent translation of the cluster, and the curved arrows denote the coherent rotation of the cluster.

3   Numerical experiments

3.1   Cluster generating

The gravitational N-body code `pkdgrav` was used for numerical experiments in this study. The code has been adapted to treat both soft-sphere and hard-sphere collisions for planetesimal modeling using a high-performance gravity-tree algorithm [10, 23].

The first group of simulations aims at generating as many different configurations as possible, in order to determine the range of structures of the cluster of the same components. We start with a disperse cloud

of 27 particles as specified in Section 2.2, which are initially dispersed in a $560\,\text{m} \times 640\,\text{m} \times 400\,\text{m}$ cuboid, and allow it to collapse under its self-gravity. The initial positions and velocities of these particles are random, subject to a given total angular momentum $\boldsymbol{L}$. For each run, the simulation is performed until the aggregate of particles settles down, i.e., an equilibrated cluster is generated. A total mass 8.24×10^6 ton and overall dimension $\sim$300 m were chosen to be representative of a small asteroid, e.g., asteroid (99942) Apophis. Three $\boldsymbol{L}$ values were used to construct the clusters: minimum angular momentum $\boldsymbol{L} = 0$ kg·m^2·s^{-1} (no spin); medium angular momentum $\boldsymbol{L} = 5.5164 \times 10^9$ kg·m^2·s^{-1} (period 9–16 h); and maximum angular momentum $\boldsymbol{L} = 1.1033 \times 10^{10}$ kg·m^2·s^{-1} (period 4–7 h), which is a high spin rate for rubble-pile asteroids in practice. 3000 clusters were generated for each $\boldsymbol{L}$ following this approach.

The created clusters with different interior structures serve our reference set, based on which we observe the connections between the structural properties and the eigenvalues' spectrum λ_i statistically. By studying these widely distributed cluster samples for three different $\boldsymbol{L}$ values, we seek a confirmation of the regimes revealed by the eigen analysis and a better understanding of the dependence of the cluster's resistance on the configuration.

3.2   Impact simulations

The reshaping processes induced by non-disruptive impacts are the focus of this study. These impacts from micrometeorites are regarded as a trivial low-energy events experienced by most asteroids larger than 100 m. Since a rubble-pile asteroid can reshape following a regime rearrangement of the constituent blocks, we reproduce these processes with numerical simulations by modeling collisional effects on the sample clusters.

In the second group of simulations, instantaneous impulses are applied to the clusters generated in Section 3.1 to mimic the impacts from moderate meteorites. Special attention is paid to the bulk reconfiguration of sample clusters, thus we ignore the details of the impact on the surface such as the cratering mechanism and the ejecta formation, although these non-catastrophic impacts are reasonably of high energy. It aims at a principle exploration, and the details of the interaction between the projectile and the asteroid's surface must be handled with care in a

subsequent discussion. The impulse is given an arbitrary direction and limited magnitude (to avoid disruption) to mimic a single impact from a micrometeorite. The impacting location is randomly chosen among the surface particles of the cluster. The traveling waves among the media of constituent blocks are numerically approximated by subsequent interactions between the particles, which is basically a principle approximation to the sound propagation because we employed parameters biased away from the rock material. The simulation continues until the cluster equilibrates again, with only two possible outcomes: an irreversible rearrangement that changes the cluster's structure; or reversion to the original configuration (i.e., a stable outcome; see Section 2.2). This process is repeated automatically for each simulation until a very robust configuration is reached for the specified impact magnitude. The interval between two impulses needs to be long enough to ensure that the cluster can settle down completely. The magnitude of the impulse is chosen based on the surface seismograms in previous research of (433) Eros's surface modification process [24] that produced a seismic wave in magnitude of 1 mm at hundreds of meters from the impact site. Thus a magnitude 1.87×10^7 kg·m·s^{-1} is used, which is very large considering the small total mass of the example cluster. It will reproduce a seismic shaking of significant magnitude at positions far from the impacted site.

A simple and efficient indicator is required to trace the reshaping processes of each cluster (tracking all the 9000 clusters using the coordinates of configuration $\boldsymbol{x}$ would be a cumbersome task). Simply measuring the semi-axes of the enclosing ellipsoid is not sufficient, because clusters of tens of particles have relatively strong shearing strength that prevents the overall shape coming to fluid equilibrium shapes. Instead, we adopt the cluster's three principal moments of inertia $[I_x, I_y, I_z]$ as indicators to quantify the clusters (in CPF), and we introduce the volume of the inertia ellipsoid V_E to indicate the degree of disorder of the particles' arrangement in the cluster, or packing density:

$$V_E = I_x I_y I_z \tag{9}$$

The third group of simulations consists of a grid search on two principal parameters, the rotational speed, i.e., $\boldsymbol{L}$, and the impact magnitude. The three clusters in Fig. 3 are representative of the simulation outcomes and cover a wide range of V_E:
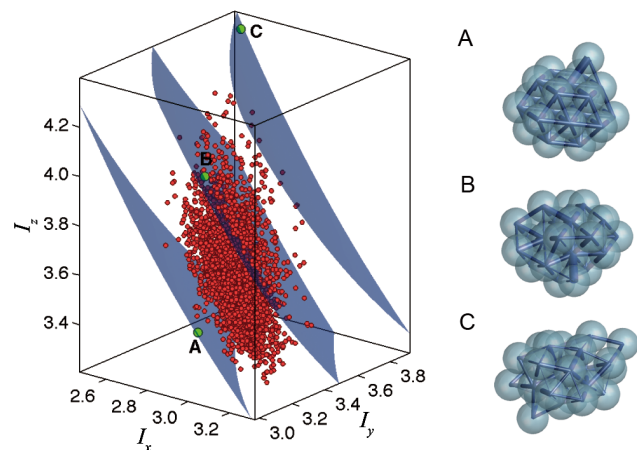
Fig. 3 Distribution of 3000 clusters with $L = 0$ in the inertia frame (unit: 10^{13} kg·m²). Each of the red solid circles indicates the three coordinates I_x, I_y, I_z of the corresponding cluster. The blue sheets indicate level surfaces of V_E, and the labeled green markers on them indicate the three sample clusters A, B, C, which are demonstrated with the snapshots on the side. The bubbles indicate the particles in the clusters A, B, and C, and the dark frameworks indicate the contacts between the particles, which are shown to illustrate their configurations.

A is 3.1512×10^{40} kg³·m⁶ (hexagonal packing), B is 3.7161×10^{40} kg³·m⁶ (moderately disordered packing), and C is 4.2806×10^{40} kg³·m⁶ (very disordered packing). For each cluster, the simulations are conducted at the nodes of a 6×6 mesh grid, which is parameterized with rotational speed from 0 to 2.67×10^{-4} rad·s⁻¹ and impact magnitude from 0 to 1.87×10^{7} kg·m·s⁻¹. For each simulation, the disturbing impacts are repeated again and again until the configuration reaches a final state that no longer responds to the impacts. The final configurations of the clusters are recorded and the changes are quantified by V_E.

4 Results

4.1 Cluster statistics

The sample clusters provide an approximation to the representative set of all possible configurations. In this section, the clusters are represented in CPF. We scale these clusters by layering their coordinates $[I_x, I_y, I_z]$ on the level surfaces of V_E, thus a basic law for the distribution is derived. Then we calculate several basic physical properties of these clusters, and by establishing connections between these properties, we show the stable indicator derived from eigen analysis is globally

valid for our experiments.

4.1.1 Distribution of $[I_x, I_y, I_z]$

Figure 3 illustrates the 3000 clusters of zero total angular momentum (minimum L) in the inertia frame. The diffuse distribution reveals the enormous number of possible configurations even for a cluster of only 27 particles, which is attributed to the multiple degrees of freedom. It is worth noticing that the ideal equilibrium structures are isolate in the coordinate system, because the static friction is omitted in our model.

V_E serves as a useful indicator for the clusters' overall shapes because it is an integral parameter that correlates with the arrangement of the cluster. In general, clusters in dense packing (low porosity) have smaller V_E than those in loose packing (high porosity). To take a detailed look at the structure of the distributed "cloud" in Fig. 3, we present three level surfaces of V_E that denote small, medium, and large values of V_E. Three clusters A, B, and C are indicated on the three respective surfaces, so that the configurations of clusters at different levels can be checked visually: cluster A in the bottom of the cloud represents almost hexagonal packing, which is a dense regular packing with a maximum volume fraction ($\sim$0.64); cluster B is on the middle layer where the cloud is heavily populated and moderately disordered; cluster C is at the sparse area at the top of the cloud; it is highly disordered and represents a prolate overall shape.

The distribution in Fig. 3 suggests that natural aggregation of boulders tends to evolve into configurations with moderate disorder, which is a hypothesis of no external disturbances based on probability. Another finding is, the cluster's extent of disorder (or porosity) grows as V_E increasing. Figure 4 shows the histograms of all three sets of clusters with different total angular momentum L (see Section 3.1). For each set, we calculate the frequency of clusters with different V_E. The clusters at minimum L present a bias-normal distribution with relatively low covariance; the medium L results in a slight positive shift of the histogram than the minimum L; and the maximum L causes a significant positive shift of the histogram and more decentralized distribution.

Figure 4 shows the probability distribution of clusters' configurations generated by randomly dispersed particles, in which the most likely outcome is neither dense packing nor loose disordered packing. This result
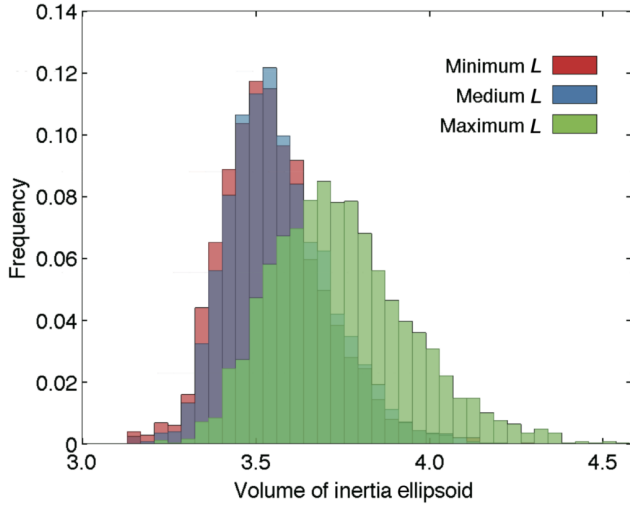
Fig. 4 Histograms of V_E for three sets of clusters with different total angular momentum clusters (unit: 10^{40} kg³·m⁶). Each set includes 3000 clusters (see Section 3.1). The red, blue, and green bars indicate the frequency of clusters at minimum, medium, and maximum L, respectively.

suggests that the most stable structure is difficult to form by once disturbance. After a dispersive impact, the reaccumulated constituents most likely form a new aggregate in sub-stable state. The very robust cluster must be created by repeated moderate disturbances, which can break all unstable links between the particles. Besides, Fig. 4 also shows the rotation plays an important role in the reshaping processes of the cluster, which will be discussed in Section 4.3.

4.1.2 Structural factors V_E, P_G, and I_S

As noted in Section 4.1.1, the structural stability (or strength) of the cluster is highly related to the arrangement of the particles, which is generally indicated by the volume of inertia ellipsoid V_E. The total gravitational potential P_G partly explains this connection, that the porous clusters (large V_E) store more energy than clusters with dense packing, which is the reason for the latter usually has better stability under external disturbances. On the other hand, the spectrum of eigenvalues λ_i also denotes the cluster's structural stability (see Section 2). We define the stability index I_S of a cluster by

$$I_S = \sum_i \mathrm{Re}\,(\lambda_i) \qquad (10)$$

which reflects the cluster's total capability to resist external disturbances. Thus we get three indicators highly correlated with the structural strength: V_E, P_G,

and I_S, which are derived separately based on different theories or simulations. Figure 5 shows the fitting curves of P_G (a) and I_S (b) varying as V_E based on 9000 sample clusters of three $\boldsymbol{L}$ values (see Section 3.1). As illustrated, P_G increases uniformly as V_E in nearly linear fashion, suggesting a monotonic connection between the interior degree of disorder and the extra potential energy restored in the cluster. I_S shows a steep increase with V_E then asymptotes when $V_E > 3.5 \times 10^{40}$ kg³·m⁶, implying a highly unstable margin where the clusters are disordered in configuration.

Unlike the P_G curves, which are almost the same at all three $\boldsymbol{L}$ values, I_S shows the influence of the total angular momentum: medium $\boldsymbol{L}$ makes not much difference, which is consistent with the probability distribution in Fig. 4, while high $\boldsymbol{L}$ leads to a significant shift down in the fitted curve, implying that high
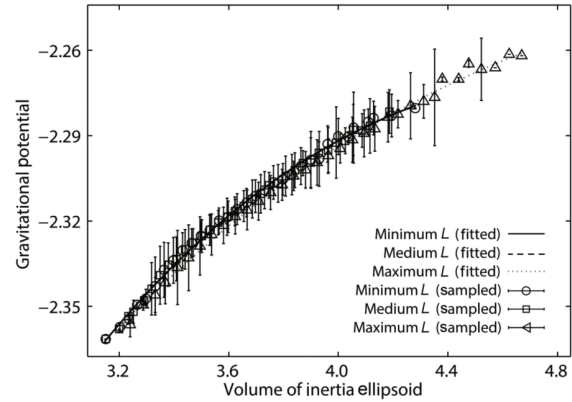
(a) Gravitational potential P_G varying as V_E
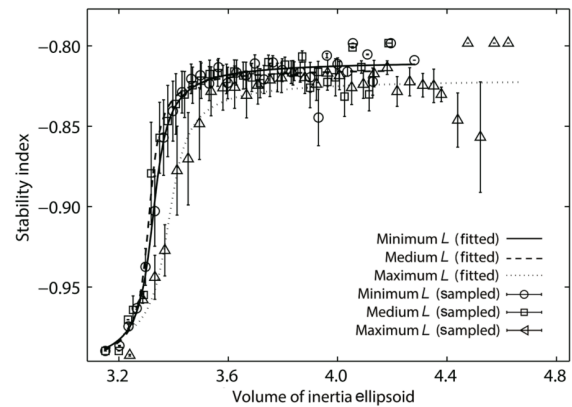
(b) Stability index I_S varying as V_E

Fig. 5 (a) Mutual gravitational potential P_G (unit: 10^7 kg·m²·s⁻²) and (b) stability index I_S (unit: s⁻¹) distribution plots of the clusters for three $\boldsymbol{L}$ values (see Section 3.1). The errorbars indicate the $1-\sigma$ deviations of the stability index at each level. The solid, dashed, and dotted lines indicate the fitted curves for the three $\boldsymbol{L}$ values.

spin rate is capable to enhance the resistance of a cluster under external disturbances. The reason is the centrifugal force partly counteracts the self-gravity of the cluster and prevents it from collapsing towards low V_E.

In summary, we find V_E, P_G, and I_S are correlated variables, which suggests they are good indicators of the cluster's structural stability, and shows the connection between structural strength and particle arrangement, namely that the strength is reduced as the interior degree of disorder increases. The rotation also plays an important role, with a high proportion of the loose disordered clusters are obtained at maximum $\boldsymbol{L}$, showing the enhancing effects of the centrifugal force. These features are fitted well with the results of a recent study on the structure of the primary of binary near-Earth asteroid (65803) Didymos [25]. In this work, they found the structured interior provides greater shear strength, which may be enough to explain the primary's fast rotation without the need for cohesion.

4.2   Structural evolution due to impacts

Figure 6(a) records the changes of $[I_x, I_y, I_z]$ for clusters of $\boldsymbol{L} = 0$ during a series of random collisional processes described in Section 3.2. All the clusters are confirmed to reach robust equilibria before 50 impacts, i.e., the fixed-magnitude impulse does not change their configurations any further. The structural evolution of each cluster is recorded and illustrated by inertia paths (Fig. 6). A common trend that can be observed among the 3000 samples is all clusters exhibit non-increasing V_E, and most exhibit a step-wise decrease in V_E. To take a detailed look at the structural changes, we highlight one of the paths and show it in the enlarged box. Four level surfaces of V_E are also included at the step values of V_E. Since the path is chosen randomly, it represents the typical mode of the structural evolution among all samples. We found a common regime that we call a "wander–jump" during these processes, that among the impacts, the very efficient ones at reducing V_E are quite rare. Between two efficient ones, most impacts just manifest as small structural perturbations at the same level surface of V_E. The small perturbations cause slight reshaping effects in narrow regions in the inertia frame, and sometimes a cyclic path on the level surface.

Figure 6(b) illustrates the variation of V_E with the number of impacts, according to the highlighted path shown in Fig. 6(a). The V_E decrease is primarily
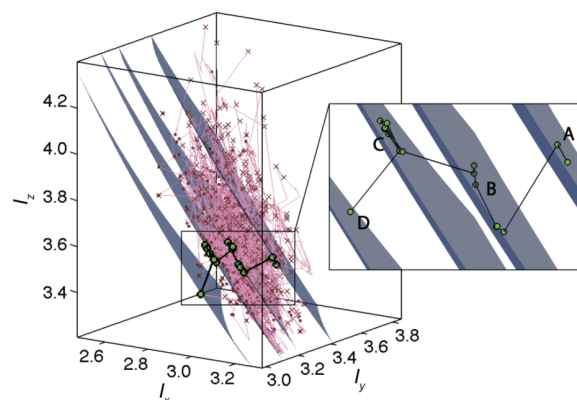
(a) Changes of the clusters' I_x, I_y, I_z due to impacts
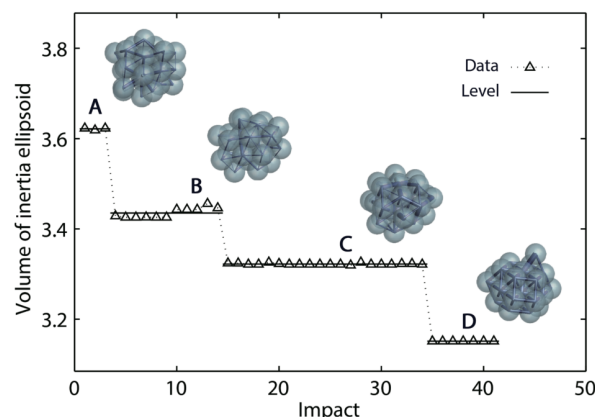
(b) Variation of V_E with the number of impacts

Fig. 6   (a) Changes of the clusters' $[I_x, I_y, I_z]$ due to impacts, based on 3000 clusters with $\boldsymbol{L} = 0$ (see Section 3.1). Fifty impacts of fixed magnitude are applied to ensure the clusters can rarely be reshaped any further. The crosses indicate the original coordinates of each cluster, and the dots indicate their final coordinates. The light solid lines indicate the paths between the original and final configurations. The dark solid line indicates a representative case among these paths, on which all the intermediate structures of the cluster are marked with solid green circles. Four blue sheets indicate the level surfaces of V_E where the cluster is at the "wander" stage, and structures on them are marked with A, B, C, D respectively, presented in an enlarged view. (b) Variation of V_E with the number of impacts for the highlighted cluster shown in (a). The triangle markers indicate V_E values at each impact, and solid lines indicate the levels of the four sets. Four bubble frameworks are shown to represent the structure of the cluster at impact 2 (set A), 11 (set B), 30 (set C), and 40 (set D).

triggered by three impacts, the 3rd, 14th, and 34th. Four isovalue sets of structures are labeled on the highlighted path respectively as A, B, C, D; each represents several structures in the "wander" stage. We choose one typical structure out of each set and present them with bubble frameworks in the figure. The structural evolution of this cluster exhibits a

clear tendency towards low V_E, i.e., low gravitational potential and small stability index (see Section 4.1.2). The arrangement of the particles trends to be more and more regular and ends up near dense hexagonal packing in set D. This variation indicates an increasing structural strength of the cluster, and Fig. 6(b) also shows an increasing number of impacts is required to further reduce V_E from set A to set D, which is numerical evidence for increasing structural strength.

Returning to rubble-pile asteroids, the results suggest the trivial non-disruptive impacts might play an important role in the rearrangement of the constituent blocks, which may strengthen these rubble piles and help to build a robust structure under impacts of similar magnitude. The dependence of structural changes on V_E can be examined by dividing up their evolution into equal bins in V_E. Figure 7 illustrates the clusters divided into five bins in V_E, showing that larger V_E values reduce more quickly in response to impacts. The histogram shows that highly disordered clusters are less capable to resist external disturbances. All the clusters are driven towards low V_E by the frequent impacts, and the final mean values for clusters in all five bins drop below 3.5×10^{40} kg^3·m^6 after the impacts, which is consistent with the criteria predicted by Fig. 5(b) (see Section 4.1.2).

Figure 8 illustrates the histograms for clusters of three L values before and after the impacts as a function of V_E. The final distributions become more concentrated compared to the original ones, while the rotation seems to partly resist the tendency towards dense packing under impacts. The mean value and covariance of these distributions as shown in Table 1.

To interpret what happens to real rubble-pile asteroids, we consider these results in light of current
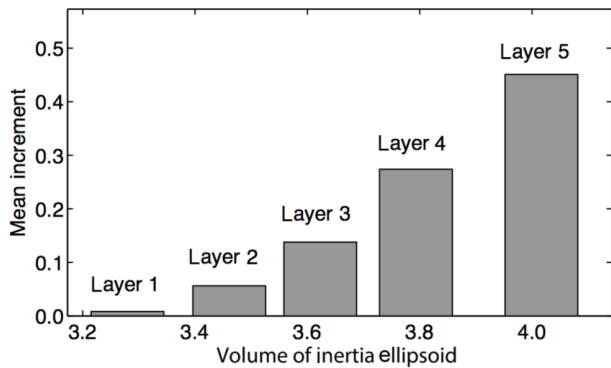
Fig. 7 Mean increment of V_E in different bins. Five bins are defined on a linear scale of V_E=3.1512, 3.3473, 3.5434, 3.7396, 3.9357, and 4.1319 (unit: 10^{40} kg^3·m^6).

(a) Minimum L

(b) Medium L
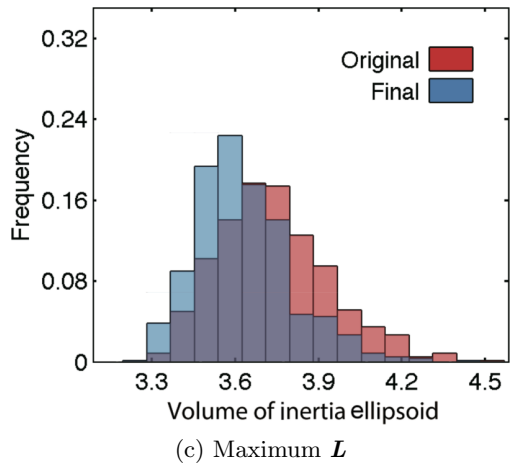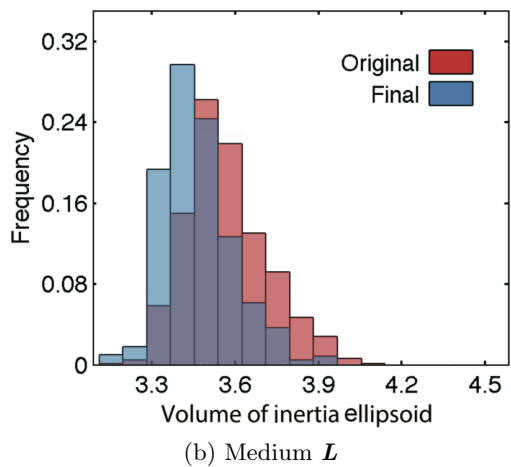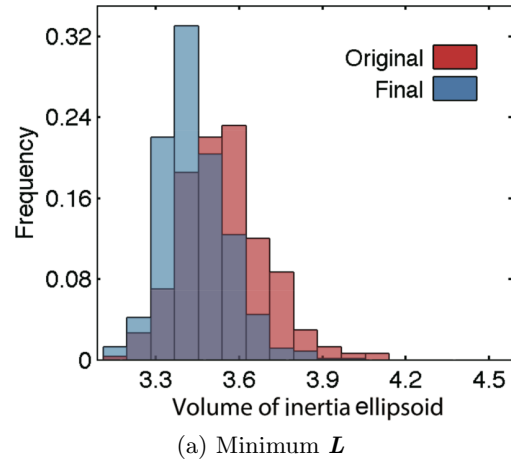
(c) Maximum L

Fig. 8 Histograms of V_E for clusters at minimum, medium, and maximum L (unit: 10^{40} kg^3·m^6). The red and blue bars indicate clusters before and after the impacts, respectively.

theories regarding the formation of rubble piles. If a rubble pile formed by reaccumulating from fragments of some catastrophic impact, it may suffer continual low-energy impacts during its subsequent evolution

Table 1 Mean value and covariance of the distributions in Fig. 8

L	State	Mean value	Covariance
Minimum	Original	3.5459	0.1536
	Final	3.4386	0.1184
Medium	Original	3.5664	0.1485
	Final	3.4641	0.1261
Maximum	Original	3.7370	0.2008
	Final	3.6251	0.1714

that result in shaking and rearrangement of the constituent blocks. The simulations show that porous structures can damp the impact energy very efficiently by reshaping to some dense packing structures with better stability. On the other hand, the total angular momentum plays a significant role during this process, for larger spin rate can prevent the porous clusters from collapsing down to dense packing, which may be one of the reasons for the fact that several fast-spin asteroids possess relatively low bulk density, such as (15) Eunomia, (45) Eugenia, (87) Sylvia, (762) Pulcova, (121) Hermione, (16) Psyche, etc. [26].

4.3 Impact parameter dependence

Figure 9 summarizes the results of a grid search on impacts. The diagram of rotational speed and impact magnitude shows the increments of V_E at 36 grid points for the three clusters. It shows these continual non-disruptive impacts do change the clusters' configurations in a common regime. The three cluster configurations A, B, C as identified in Section 4.1.1 are employed. Generally, the dense packing cluster A shows greater robust stability than disordered clusters B and C at all grid nodes, i.e., the changes of V_E for A are much

smaller than those for B and C. Rotation proves to be a significant factor in influencing the reshaping effects, as indicated by the fact that the increment of V_E decreases as the rotational speed increases, which is quite apparent in Fig. 9 for the porous cluster C. It also confirms that more porous interiors may exist among fast-rotating rubble piles compared to the slow-rotating ones, as stated in Section 4.2. Also, as the impact magnitude increases, the increment of V_E grows for all the three clusters. In particular, we find a magnitude criterion around 1.13×10^7 kg·m·s^{-1} below which all the clusters are almost immune to the impacts. The figure is also consistent with the eigen analysis, for the theory predicts the existence of a stable margin, i.e., below some magnitude all disturbances around equilibrium can be recovered from eventually.

As an aside, the numerical experiments in this paper are all based on an oversimplified model (soft-sphere clusters) and somewhat arbitrary setup of parameters, which are far from enough to mimic a real astronomical scenario. We present the results as a representation of some qualitative rules, which is a bridge to understanding the common driving mechanisms during the evolution of rubble-pile asteroids.

5 Conclusions

In this paper, eigen analysis was introduced to study the structural stability of equilibrated soft-sphere clusters, serving as a representative model for rubble-pile asteroids, so that the strength of a cluster and its responses to external disturbances can be estimated just from its configuration. Further, the results were applied
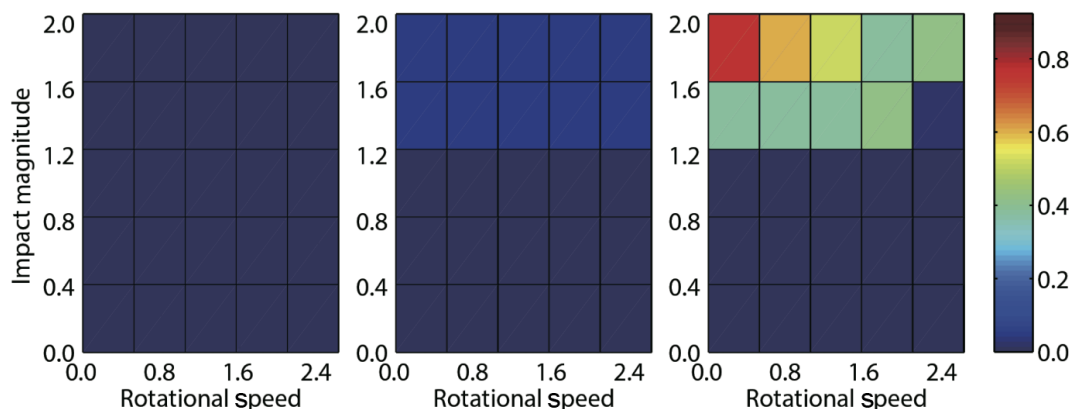
Fig. 9 Colormap of the increment of V_E for three sample clusters, based on the results from gridded simulations parameterized by rotational speed (unit: 10^{-4} rad·s^{-1}) and impact magnitude (unit: 10^7 kg·m·s^{-1}). The three clusters demonstrated in Fig. 3 are used: cluster A (left), cluster B (middle), and cluster C (right). A uniform colormap shows the increment of V_E in 10^{40} kg^3·m^6.

TSINGHUA UNIVERSITY PRESS Springer

to the analysis of the impact responses of clusters, to explore the dependence of rubble-pile asteroids' reshaping process on the interior structure. Numerical experiments were designed to test our theoretical predictions and to reveal the particular forms of this dependence.

The eigen analysis shows that the eigenvalues λ_i of the equilibrated cluster system indicate its stability to specific types of external disturbances, and corresponding reshaping patterns can be determined using the associated eigenvectors ϕ_i. Simulations were performed to confirm this finding numerically.

Randomly generated clusters provided a representative region of possible configurations, with the results showing that the volume of inertia ellipsoid $V_{\rm E}$ is a significant parameter for clusters since it largely measures the degree of disorder of the constituents' arrangement. Statistically, we find the stability index $I_{\rm S}$, total gravitational potential $P_{\rm G}$, and $V_{\rm E}$ are always consistent, and discussed the dependence of the structural stability on these parameters based on analysis of the sample clusters.

Simulations of the reshaping processes of clusters under non-dispersive impacts reveal a common regime for the structural changes, which we called "wander–jump", i.e., the progenitors formed by reaccumulation of initial violent catastrophic impacts may not have very stable interior structures, and a series of collapses triggered by subsequent continual low-energy impacts from small fragments will change the constituents' arrangement gradually towards a dense packing, in a secular geological process. Using the soft-sphere cluster model, we show that when the repeated impacts reach some critical magnitude, the configurations of the samples will evolve consistently towards crystallization after long enough (for equal-sized spheres, the crystallization is hexagonal packing).

A grid search was performed to identify the parameter dependence of the reshaping effects, showing that the dense packing cluster has the best structural stability among all the samples. The rotational speed proves to play an important role for it exhibits an enhancing effect on loose-packed clusters, i.e., the centrifugal force partly counteracts the self-gravity and keeps the porous clusters in robust equilibrium, which might explain in part why several fast-spinning asteroids have rather low bulk density. The simulations also suggest a critical magnitude exists, below which all the clusters become immune to external disturbances in any form, consistent with the prediction of the existence of a stable margin from eigen analysis.

Acknowledgements

References

[1] Richardson, D. C., Leinhardt, Z. M., Melosh, H. J., Bottke Jr., W. F., Asphaug, E. Gravitational aggregates: Evidence and evolution. In: *Asteroids III*. Bottke Jr., W. F., Cellino, A., Paolicchi, P., Binzel, R. P. Eds. The University of Arizona Press, **2002**: 501–515.

[2] Bottke Jr., W. F., Richardson, D. C., Michel, P., Love, S. G. 1620 Geographos and 433 Eros: Shaped by planetary tides. *The Astronomical Journal*, **1999**, 117(4): 1921–1928.

[3] Solem, J. C., Hills, J. G. Shaping of Earth-crossing asteroids by tidal forces. *The Astronomical Journal*, **1996**, 111(3): 1382–1387.

[4] Chapman, C. R. Asteroid collisions, craters, regolith, and lifetimes. In: *Asteroids: An Exploration Assessment. NASA Conference Publication 2053.* Morrison, D., Wells, W. C. Eds. NASA, **1978**: 145–160.

[5] Weissman, P. R. Are cometary nuclei primordial rubble piles? *Nature*, **1986**, 320: 242–244.

[6] Benz, W., Asphaug, E. Catastrophic disruptions revisited. *Icarus*, **1999**, 142(1): 5–20.

[7] Michel, P., Benz, W., Tanga, P., Richardson, D. C. Collisions and gravitational reaccumulation: Forming asteroid families and satellites. *Science*, **2001**, 294(5547): 1696–1700.

[8] Asphaug, E., Benz, W. Density of comet Shoemaker–Levy 9 deduced by modelling breakup of the parent "rubble pile". *Nature*, **1994**, 370: 120–124.

[9] Chodas, P. W., Yeomans, D. K. The orbital motion and impact circumstances of Comet Shoemaker–Levy 9. In: The Collision of Comet Shoemaker–Levy 9 and Jupiter, IAU Colloquium 156. Proceedings of the Space Telescope Science Institute Workshop. Noll, K. S., Weaver, H. A., Feldman, P. D. Eds. Cambridge University Press, **1995**: 1–30.

[10] Richardson, D. C., Bottke Jr., W. F., Love, S. G. Tidal distortion and disruption of Earth-crossing asteroids. *Icarus*, **1998**, 134(1): 47–76.

[11] Ballouz, R.-L., Richardson, D. C., Michel, P., Schwartz, S. R., Yu, Y. Numerical simulations of collisional disruption of rotating gravitational aggregates: Dependence on material properties. *Planetary and Space Science*, **2014**, 107: 29–35.

[12] Bottke Jr., W. F., Richardson, D. C., Love, S. G. Can tidal disruption of asteroids make crater chains on the Earth and Moon. *Icarus*, **1997**, 126(2): 470–474.

[13] Farinella, P., Paolicchi, P. Triaxial equilibrium ellipsoids among the asteroids. *Icarus*, **1981**, 46(1): 114–123.

[14] Kryszczyńska, A., La Spina, A., Paolicchi, P., Harris, A. W., Breiter, S., Pravec, P. New findings on asteroid spin-vector distributions. *Icarus*, **2007**, 192(1): 223–237.

[15] Richardson, D. C., Elankumaran, P., Sanderson, R. E. Numerical experiments with rubble piles: Equilibrium shapes and spins. *Icarus*, **2005**, 173(2): 349–361.

[16] Asphaug, E. Similar-sized collisions and the diversity of planets. *Chemie der Erde-Geochemistry*, **2010**, 70(3): 199–219.

[17] Tanga, P., Comito, C., Paolicchi, P., Hestroffer, D., Cellino, A., Dell'Oro, A., Richardson, D. C., Walsh, K. J., Delbo, M. Rubble-pile reshaping reproduces overall asteroid shapes. *The Astrophysical Journal*, **2009**, 706(1): 197–202.

[18] Sánchez, P., Scheeres, D. J. Simulating asteroid rubble piles with a self-gravitating soft-sphere distinct element method model. *The Astrophysical Journal*, **2011**, 727(2): 120–133.

[19] Schwartz, S. R., Richardson, D. C., Michel, P. An implementation of the soft-sphere discrete element method in a high-performance parallel gravity tree-code. *Granular Matter*, **2012**, 14(3): 363–380.

[20] Perko, L. *Differential Equations and Dynamical Systems*. Springer-Verlag New York, **2001**.

[21] Wiggins, S. *Introduction to Applied Nonlinear Dynamical Systems and Chaos*. Springer-Verlag New York, **2003**.

[22] Shilnikov, L. P., Shilnikov, A. L., Turaev, D. V., Chua, L. O. *Methods of Qualitative Theory in Nonlinear Dynamics*. World Scientific Publishing Co. Pte. Ltd., **1998**.

[23] Stadel, J., Wadsley, J., Richardson, D. C. High performance computational astrophysics with PKDGRAV/gasoline. In: *High Performance Computing Systems and Applications*. Dimopoulos, N. J., Li, K. F. Eds. Springer US, **2002**: 501–523.

[24] Richardson, J. E., Melosh, H. J., Greenberg, R. Impact-induced seismic activity on Asteroid 433 Eros: A surface modification process. *Science*, **2004**, 306(5701): 1526–1529.

[25] Zhang, Y., Richardson, D. C., Barnouin, O. S., Maurel, C., Michel, P., Schwartz, S. R., Ballouz, R.-L., Benner, L. A. M., Naidu, S. P., Li, J. Creep stability of the proposed AIDA mission target 65803 Didymos: I. Discrete cohesionless granular physics model. *Icarus*, **2017**, 294: 98–123.

[26] Britt, D. T., Yeomans, D., Housen, K., Consolmagno, G. Asteroid density, porosity, and structure. In: *Asteroids III*. Bottke Jr., W. F., Cellino, A., Paolicchi, P., Binzel, R. P. Eds. University of Arizona Press, **2002**: 485–500.

Yang Yu is now an associate professor (tenure track) at Beihang University in Beijing, China. He joined the School of Aeronautic Science and Engineering in April 2016. He obtained his B.S. degree in physics from Beihang University (2009) and Ph.D. degree in aeronautics & astronautics from Tsinghua University (2014). He had his postdoctoral position at Observatoire de la Côte d'Azur in France (2014–2016). His research interests include the Hamiltonian dynamics of celestial systems and the formation and evolution of minor planets. E-mail: yuyang.thu@gmail.com.